Journal of Materials Chemistry B

ROYAL SOCIETY OF CHEMISTRY

PAPER

View Article Online
View Journal | View Issue

Cite this: J. Mater. Chem. B, 2022, 10, 2544

Accelerated tissue regeneration in decellularized vascular grafts with a patterned pore structure

Atsushi Mahara,[a] Kentaro Kojima,[ab] Masami Yamamoto,[ac] Yoshiaki Hirano[b] and Tetsuji Yamaoka *[a]

Received 18th October 2021,
Accepted 11th November 2021

DOI: 10.1039/d1tb02271g

rsc.li/materials-b

Decellularized tissue is expected to be utilized as a regenerative scaffold. However, the migration of host cells into the central region of the decellularized tissues is minimal because the tissues are mainly formed with dense collagen and elastin fibers. This results in insufficient tissue regeneration. Herein, it is demonstrated that host cell migration can be accelerated by using decellularized tissue with a patterned pore structure. Patterned pores with inner diameters of 24.5 ± 0.4 μm were fabricated at 100, 250, and 500 μm intervals in the decellularized vascular grafts *via* laser ablation. The grafts were transplanted into rat subcutaneous tissue for 1, 2, and 4 weeks. All the microporous grafts underwent faster recellularization with macrophages and fibroblast cells than the non-porous control tissue. In the case of non-porous tissue, the cells infiltrated approximately 50% of the area four weeks after transplantation. However, almost the entire area was occupied by the cells after two weeks when the micropores were aligned at a distance of less than 250 μm. These results suggest that host cell infiltration depends on the micropore interval, and a distance shorter than 250 μm can accelerate cell migration into decellularized tissues.

1. Introduction

Decellularized blood vessels have been developed as an extracellular matrix for tissue-engineered vascular grafts.[1,2] The graft is expected to be infiltrated by the host cells after transplantation and regenerate the vascular tissue in the host body.[3] However, a major limitation of the use of acellular scaffolds is that cell ingrowth is restricted by the dense fibril microenvironment (collagen, elastin, and glycosaminoglycan).[4] When host cells migrate into the acellular tissue, the matrix is degraded by immune cells such as macrophages and T helper 2 cells.[5,6] The long-term accumulation of excess inflammatory macrophages induces serious immune rejection and incomplete regeneration.[6,7] Given these considerations, rapid infiltration of host cells into the decellularized tissue would be a very effective strategy for tissue regeneration and suppression of undesirable inflammatory reactions.

To this end, porous scaffolds have been investigated. In the case of polyurethane (PU) vascular grafts, methods of fabricating perforated scaffolds and the *in vivo* response have been reported by many groups.[8–10] Doi *et al.* demonstrated that a PU graft with a pore size of 100 μm, combined with growth factor, accelerated perianastomotic and transmural tissue ingrowth.[10] The immune response and *in vivo* migration of cells to porous scaffolds have been investigated using an electrospun vascular scaffold.[11,12] Wan *et al.* reported that the pore size and scaffold thickness in the electrospun scaffold regulated the macrophage phenotype and remodeling process.[11] In the case of synthetic polymer scaffolds, the pore size and distribution can be easily controlled. In contrast, investigations of the porous structure of decellularized vascular scaffolds are limited. Vascular tissue perforated by microneedling was reported to retain the cells inside the graft wall with a hydrogel.[1,13] In this case, the pore sizes and intervals were not well controlled. Bergmeister *et al.*[15] developed a decellularized vascular graft with controlled pores of 50 μm in diameter using a Ti–sapphire laser. Rapid recellularization was confirmed at six weeks. Although controlled pore structures in decellularized vascular grafts have been reported, the effect of the patterned pore structure in decellularized vascular grafts on cell infiltration, macrophage response, and tissue regeneration *in vivo* has not been investigated.

In our previous study, we developed a peptide-modified acellular graft.[16–18] The graft (length: 20–30 cm; inner diameter: 2 mm), was transplanted into the femoral artery of minipigs as a bypass graft, and the graft patency was successfully

[a] Department of Biomedical Engineering, National Cerebral and Cardiovascular Center Research Institute, Kishibe-shin Machi, Suita, Osaka 564-8565, Japan. E-mail: yamtet@ncvc.go.jp; Fax: +81-6-6170-1702; Tel: +81-6-6170-1070 ext. 31009
[b] Faculty of Chemistry, Materials and Bioengineering, Kansai University, 3-3-35 Yamatecho, Suita, Osaka 565-8680, Japan
[c] Faculty of Medical Engineering, Suzuka University of Medical Science, Suzuka, Mie 510-0293, Japan

demonstrated.[18] In this experiment, the luminal surface of the graft was covered with cells one week after transplantation. Although the cell layer formed stably at three weeks after transplantation, cell infiltration into the medium layer of the graft was minimal during the experimental period.

In this study, we employ a femtosecond laser ablation process for fabricating patterned pore structures in decellularized vascular grafts. It is hypothesized that the patterned pore structure can improve cell migration and tissue regeneration in decellularized tissues. Using the laser ablation process, micropores with controlled pore sizes and intervals are fabricated on the luminal surface of the graft. The vascular grafts are transplanted into rat subcutaneous tissues, and the cell migration and macrophage responses are evaluated. It is demonstrated that patterned pore structures with intervals smaller than 250 μm accelerate cell infiltration and tissue regeneration.

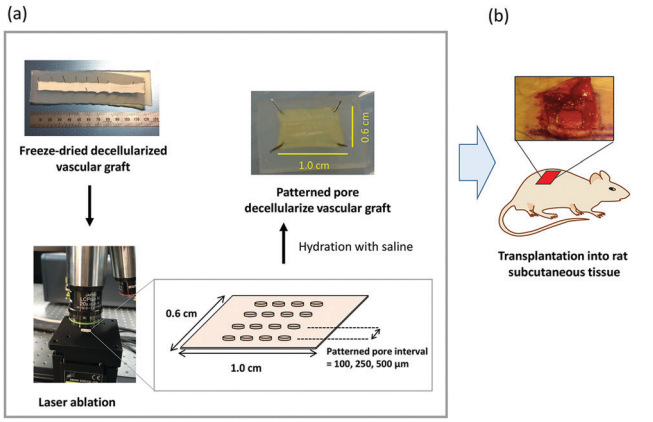

Fig. 1 Schematic representation of *in vivo* cell infiltration of pore-patterned decellularized vascular graft using rat subcutaneous transplantation model. (a) Laser ablation process applied to decellularized vascular graft, (b) the grafts were transplanted into rat subcutaneous tissue.

2. Experimental

2.1 Decellularized tissue

Ostrich carotid arteries (African black, Shimizu-Laboratory Supplies Co., Ltd, Kyoto, Japan) were purchased from Shimidzu Experimental Animal (Kyoto, Japan). Decellularization was accomplished using previously reported procedures.[18] Briefly, the ostrich carotid artery was decellularized with high hydrostatic pressure (HHP) using a cold isostatic pressurization machine (Dr Chef; Kobelco, Kobe, Japan). The pressure was increased to 980 MPa at a rate of 65.3 MPa min^{-1} and then maintained within the chamber for an additional 10 min. After pressure treatment, the tissues were washed with saline containing 40 U ml^{-1} of DNase I (Roche Applied Science, Indianapolis, IN, USA), 20 mM $MgCl_2$, and antibiotics for 3 d at 37 °C. After washing, the tissue was immersed in saline containing ethylenediaminetetracteic acid (EDTA) and antibiotics for 3 d at 37 °C to remove the remaining DNase I. After changing the solution, the decellularized tissue was preserved in the same solution until experimental use.

2.2 Fabrication of patterned pore structure

Three types of patterned pore decellularized grafts were prepared for *in vivo* evaluation (Fig. 1). Decellularized tissue with respective lengths of 1.0 and 0.6 cm was fixed on the silicon plate. The fixed tissues were immersed in 50, 70, 80, 90, 95, and 100% EtOH aqueous solution for water deprivation (dehydration). After replacing the solvents in which the tissues were immersed with *t*-butyl alcohol, the tissues were lyophilized and are hereinafter referred to as NP-grafts. The patterned pore structure was fabricated using a femtosecond laser micronanomachining system (Tokyo Instruments Inc., Tokyo, Japan). For the fabrication process, the laser power, pulse width, wavelength, and working distance were tuned to 650 mW, 300 fs, 1028 nm, and 83 pw, respectively. Other settings and fabrication conditions were in accordance with the manufacturer's instructions. After micropore fabrication, the tissues were immersed in 100, 95, 90, 80, 70, and 50% EtOH solution for 20 min under each condition. Finally, the tissue was immersed in a saline solution for 20 min to replace the solvent. The pore-patterned grafts with pore intervals of 500, 250, and 100 μm are referred to as P500-, P250-, and P100-graft, respectively. The rehydrated tissues were preserved at 4 °C until further use.

2.3 SEM images

The morphology of the patterned pores was observed by scanning electron microscopy (SEM; JCM-5700, JEOL Ltd., Tokyo, Japan). To prepare the samples for SEM observation, the samples were fixed with 1% glutaraldehyde solution (Wako Pure Chemical Industries, Ltd, Osaka, Japan). The samples were dehydrated with ethanol, immersed in *t*-butyl alcohol, and dried under vacuum. The luminal surface was coated with a gold layer in an ion coater (IB-3 ion coater, Eiko Engineering, Ibaraki, Japan) and observed using a JCM 5700 microscope.

2.4 Transplantation

All animal experiments were conducted in accordance with the Guidelines for Animal Experiments established by the Ministry of Health, Labor, and Welfare of Japan and by the National Cerebral and Cardiovascular Center Research Institute in Japan. The protocol was approved by the Committee on the Ethics of Animal Experiments of the National Cerebral and Cardiovascular Center Research Institute (Permit Number: 009017). Male Sprague Dawley rats (7 weeks old; Japan SLC, Inc., Shizuoka, Japan) were anesthetized with 2.5% isoflurane (Pfizer Japan, Tokyo). Tissue samples with areas of 1.0 and 0.6 cm^2 were subcutaneously transplanted (n = 3). The luminal surface of the tissues was placed in contact with the muscle layer, and the grafts were sutured at the edge with 6-0 Prolene (Ethicon, Somerville, NJ). The samples were extirpated at one, two, and four weeks after transplantation.

2.5 Histostaining

The cell infiltration depth and area of infiltration into the graft were evaluated by hematoxylin and eosin (HE) staining and

immunobiological staining. The specimens were fixed with 10% neutral-buffered formalin solution and immersed in a 20% sucrose solution. The specimens were then embedded in Tissue-Tek O.C.T compound (Sakura Fineteck, Tokyo, Japan) and frozen in liquid nitrogen. Frozen sections with a thickness of 7 μm were obtained using a Leica CM1860 cryomicrotome (Leica Biosystems Nussloch GmbH, Germany). Eosin and hematoxylin solutions were purchased from Fujifilm Wako Chemical (Tokyo, Japan), and staining was carried out according to the manufacturer's instructions.

The infiltration of macrophage and fibroblast cells was evaluated by staining with anti-CD68 and anti-P4HB antibodies, respectively. The sections were immersed in 95% EtOH solution for 30 min at 4 °C. A heat-mediated antigen-retrieval technique in which the sample was incubated and boiled for 20 min in 0.01 M citrate buffer at pH 6.0 was used. After cooling, the sections were washed with Tris-buffered saline/Tween 20 (TBST), pH7.4 and with phosphate buffered saline (PBS). The primary antibodies for the macrophages and fibroblasts were mouse anti-rat CD68 (Gene-Tex, San Antonio, TX, USA) at 1 : 500 dilution in PBS, and anti-P4HB antibody (Acris Antibodies GmbH, Hiddenhausen, Germany) at 1 : 200 dilution in PBS, respectively. Simple Stain Rat Max-PO (Nichirei Bioscience Inc., Tokyo, Japan) was used as the secondary antibody. The tissues were immersed overnight with primary antibodies at 4 °C. After washing with TBST, the tissues were immersed in the secondary antibody for 30 min, followed by incubation with horseradish peroxidase solution (VectorStain ABC kit, Vector Laboratories, Inc., Burlingame, CA) for 30 min at 37 °C. Diaminobenzene was applied to detect positively stained cells, and the slides were counterstained with hematoxylin.

2.6 Quantification of cell infiltration area

The cell infiltration depth and area were quantified by hematoxylin and eosin staining. The area was analyzed using ImageJ software (ver 1.5i).[19] The image size of 636 μm in length and 849 μm in width were evaluated. The medium layer of the transplanted graft was traced as the dotted white line. The edges of the infiltrated cells were traced as the dotted yellow line. The direct distance between the borderline of the medium layer at the muscle layer side and the edge of the infiltrated cells was measured as the cell infiltration distance. The cell infiltration depth is defined as the ratio of the cell infiltration distance to the medium layer thickness. The cell migration area into the medium layer was calculated, then the cell infiltration area is defined as the ratio of the area migrated by cells to the area of the medium layer. The average and standard deviation of the ratio were calculated from the three images in each sample.

2.7 Statistical analysis

The quantitative data are expressed as the mean ± standard deviation. The data were analyzed using one-way ANOVA, followed by Tukey's honest significant difference *post hoc* test assuming equal variance.

3. Results

3.1 Morphology of patterned pore structure

The patterned pore structure in the decellularized tissue was observed by SEM (Fig. 2a–c). The pores were aligned with constant intervals, and the diameter was 24.5 ± 0.4 μm (Fig. 2d and e). These images indicate that laser ablation of the decellularized tissue resulted in minimal thermal stress, enabling the fabrication of a controlled pore structure. When the laser power and pulse width in the fabrication process were not optimized, the edge of the micropore was denatured by thermal stress (data not shown). The depth of the pore was approximately 200 μm, and the media layer of the graft was completely penetrated (Fig. 2f).

3.2 Graft transplantation

The grafts were transplanted into the subcutaneous tissues of rats. After one, two, and four weeks, the grafts were observed (Fig. 3). In all cases, microvascular networks developed around the graft up to two weeks after transplantation (Fig. 3a and b). After four weeks, the microvessel number was clearly decreased only in the case of the P250- and P100-grafts, as compared with the other grafts (Fig. 3c).

3.3 Effect of patterned pore structure on cell infiltration

The cell infiltration into the patterned pore-decellularized graft was evaluated. The transplanted grafts were stained with haematoxylin and eosin (Fig. 4).

In the case of the NP-graft, a few cells were shallowly infiltrated into the media layer of the graft at one week. Four weeks after transplantation, half of the medium layer was occupied by the infiltrated cells, and the cells reached only half the depth of the medium layer. In contrast, the patterned pores in the P100-, P250-, and P500-graft were occupied with

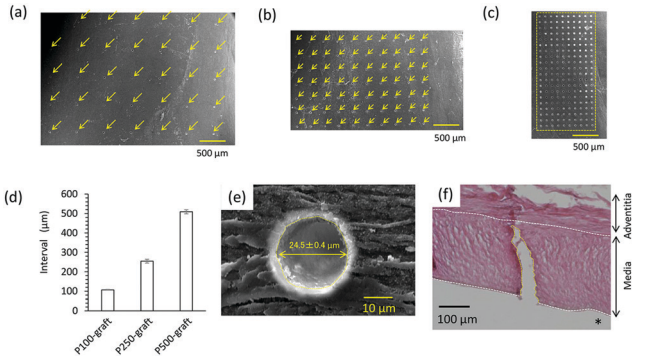

Fig. 2 Patterned pore structure in decellularized vascular graft. (a–c) SEM images of patterned pore structure on luminal surface of decellularized vascular graft. The intervals of the pores in P500-, P250-, and P100-graft were set as (a) 500, (b) 250, and (c) 100 μm, respectively. (d) Measured intervals of the patterned pores in P100-graft, P250-graft, and P500 graft are indicated. The data indicates the average (n = 10) ± S.D. Asterisks indicate a significant difference ($p < 0.01$). (e) Top-view of the pore as observed by SEM. (f) Cross-sectional image of micropore in decellularized vascular graft. The tissue was stained by HE. Asterisk indicates the luminal side.

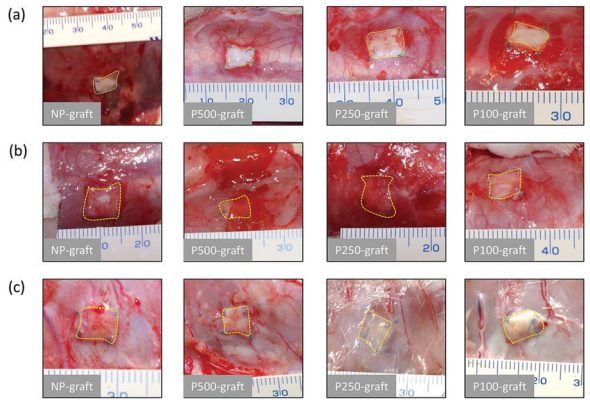

Fig. 3 Gross appearance of transplanted grafts on the subcutaneous tissue. NP, P100, P250, and P500-grafts were transplanted to subcutaneous tissue of rats for (a) 1, (b) 2, and (c) 4 weeks. The dotted yellow line indicates the transplanted grafts.

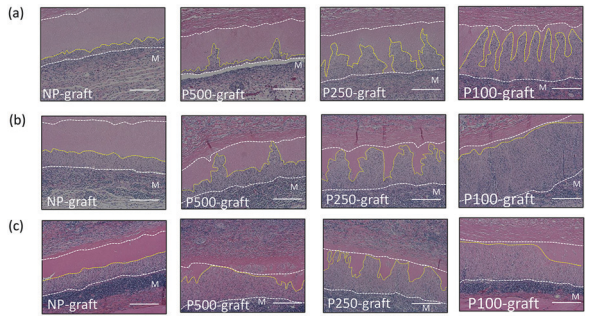

Fig. 4 HE staining images of pore-patterned decellularized vascular graft. (a) 1, (b) 2, and (c) 4 weeks after transplantation. M indicates the muscle layer side. Scale bars indicate 200 μm. The dotted yellow line indicates the edge of the migrated cells in the medium layer.

cells one week after transplantation. After two and four weeks, the cells at the pores moved in the circumferential direction, and the medium layer of these grafts was occupied by the cells. In the case of the P100-graft, the overall area of the medium layer was replaced by the host cells.

The cell infiltration depth and area were quantified as a function of the transplantation duration (Fig. 5).

In the case of the NP-graft, the medium layers were gradually replaced by the host cells, and the cells infiltrated from the luminal layer to a depth of 15% to 48% of the medium layer thickness 1 to 4 weeks after transplantation, respectively. The cell-infiltrated area at the medium layer also increased from 12% to 50% after one- and four-week transplantation, respectively. These results indicate that four weeks were required to replace almost half of the medium layer by the host cells in the case of the non-porous grafts.

In the case of the P100-, P250-, and P-500-grafts, the cells migrated 70% to 84% from the luminal surface to the outer side *via* the pores one week after transplantation. The cells then gradually moved and reached the external elastic membrane after four weeks. In contrast, the cell-infiltrated area was

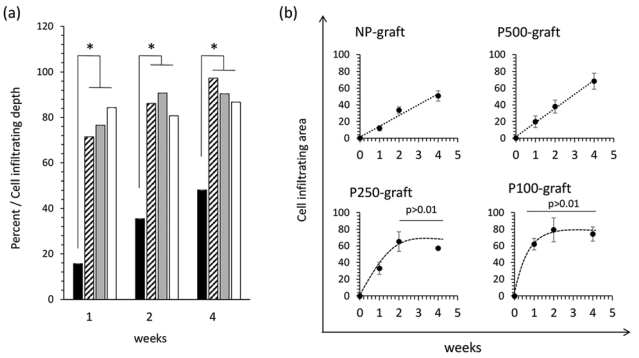

Fig. 5 Cell infiltration depth and infiltration area for pore-patterned decellularized graft. (a) Cell infiltration depths in NP, P100, P250, and P500-grafts are indicated as filled, hatched, grey, and open bars, respectively. The grafts were transplanted for 1, 2, and 4 weeks. (b) Cell infiltration area *vs.* transplantation time. The image size of 636 μm in length and 849 μm in width were used for the calculation of cell infiltrating depth and area. The average and standard deviation of the ratio were calculated from the three images in each sample.

dependent on the pore intervals. The infiltrated area gradually increased in the P500-graft, and reached almost 80% after four weeks. In the case of the P250- and P100-grafts, the infiltrated area reached a plateau after two weeks.

3.4 Host cell response

The response of the host tissue to the pore-patterned graft was evaluated by immunostaining with anti-CD68 and anti-P4HB antibodies, which were used as markers for macrophage and fibroblast cells, respectively. In the case of the NP-graft, few CD68 positive cells were present in the cell-infiltrated area at one week. Thereafter, the number of cells increased, and many CD68-positive macrophages accumulated four weeks after transplantation (Fig. 6). In contrast, many CD68 positive cells were observed in the P-500 graft one week after transplantation. Although many cells were observed after two weeks, the number of cells decreased significantly at four weeks. In the case of the P250 and P100-grafts, few CD68 positive cells were observed

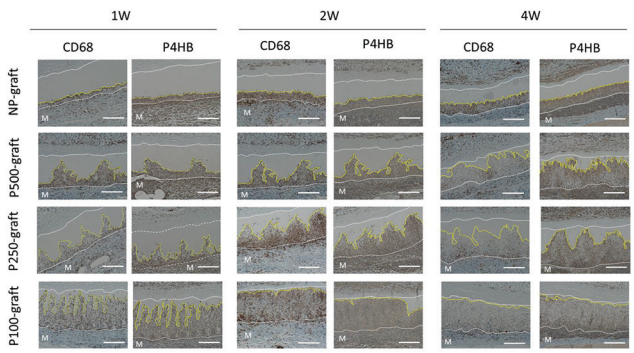

Fig. 6 Macrophage and fibroblast response to pore-patterned decellularized graft. The grafts were transplanted for 1, 2, and 4 weeks. Fibroblast cells and macrophages were stained with anti-P4HB and anti-CD68 antibodies, respectively. M indicates the muscle layer side. Scale bars indicate 200 μm. The dotted yellow line indicates the edge of the migrated cells in the medium layer.

at one week. The number increased significantly at two weeks. Four weeks after transplantation, very few CD68-positive macrophages were observed in these tissues.

The accumulation of fibroblast cells was evaluated by anti-P4HB antibody staining. At two weeks, many cells in the cell infiltrating area expressed the P4HB marker in all cases. In the case of the NP-, P500- and P250-grafts, the expression in the central region of the cell-infiltrated area was weak at four weeks. Four weeks after transplantation of the P100-graft, very few P4HB positive cells were observed in the cell-infiltrated areas. In contrast, numerous P4HB positive cells were observed in the NP-graft at four weeks.

4. Discussion

Decellularized tissue scaffolds are expected to be biodegradable matrices. However, acellular tissues are formed with dense connective tissues, such as collagen and elastin. Matrix degradation and replacement with host cells is largely restricted by the structure. Herein, the prospective of cell migration to a pore-patterned decellularized vascular graft and rapid tissue regeneration were investigated. It has been reported that perforated skin,[20,21] nerves,[22,23] trachea,[24] temporomandibular joint discs,[25] and bone grafts[26] have been fabricated on collagen and decellularized scaffolds. These data suggest that cell migration and tissue regeneration are improved by microporous structures. However, few studies have evaluated the effect of a patterned pore structure on cell infiltration and macrophage response in acellular grafts. In this study, a patterned pore structure was fabricated in a decellularized vascular graft by the femtosecond laser ablation process, and the *in vivo* cell migration and macrophage response were evaluated.

It is difficult to fabricate controlled micropores in acellular tissues because of the soft materials. Microneedling or laser perforation techniques have been used for fabricating micropores on naturally-derived scaffolds.[13–15,27] Microneedling is easy to handle, and micropores can be fabricated along the long-axis direction of the vascular grafts.[13] The major advantage of this process is that cell and/or growth factors are delivered to the inside of the decellularized tissue through the needle. However, it is difficult to fabricate fine and aligned porous structures in acellular tissues by needling. In contrast, the machine-assisted laser fabrication process is highly superior for fabricating size- and interval-controlled micropores in tissues. Zhou *et al.* fabricated a porous decellularized trachea scaffold using laser fabrication techniques.[24,28] They successfully fabricated pores with a diameter of 810 μm evenly in the decellularized trachea at intervals of 1 mm.[24] Decellularized vascular grafts having laser-machined micropores with a diameter of 50 μm and a density of 50 pores cm^{-2} have been reported.[15] Therefore, laser processing techniques for fabricating pores are promising for improving cell migration and rapid tissue remodeling. Herein, patterned pore structures with small diameters and uniform intervals were successfully fabricated in decellularized vascular grafts using femtosecond laser ablation (Fig. 2). The patterned pore structure with a two-dimensional distribution is a desirable matrix for controlling recellularization and tissue regeneration.

The immune response of the host to biological scaffold materials is different from the response to synthetic materials and depends on the origin of the tissue and fabrication process.[7] It has been reported that the host response to decellularized tissue is active until approximately two weeks after transplantation.[6] Herein, microvessel accumulation was observed around the graft, and the degree and duration were largely dependent on the patterned pore structure up to four weeks (Fig. 3). After four weeks of transplantation, the microvessels clearly receded only in the case of the P250 and P100-graft. In the acute immune response, the macrophages accumulate around the graft and secrete some cytokines. Following this reaction, the major response mainly switches to the fibroblast accumulation.[29] In this study, the macrophage and fibroblasts were evaluated for evaluation of major immune response. As shown in Fig. 5b, the cell infiltrated area in the P250 and P100-grafts reached a plateau at two weeks, and the number of CD68 positive cells decreased significantly at four weeks (Fig. 6). These data indicate that the acute immune response can be rapidly stabilized by accelerating host cell migration through the patterned pore structure. Juran *et al.* reported that engineered micropores with a diameter of 120 μm enhanced cellular integration in the deep part of decellularized tissue.[25] It was reported that perforation of the decellularized trachea and pericardial tissue improved the cell adherence rate.[28,30] The present study also confirmed rapid infiltration of host cells into the central region of the graft (Fig. 4 and 5a). Although cell migration and adhesion in perforated decellularized tissue have been discussed by some groups, the acute immune response to the patterned pore structure in decellularized tissues has been scarcely discussed. From the present data and prior studies, it is deduced that cell accumulation can be controlled not only by the pore size, but also by the intervals of the micropores. Thus, tissue regeneration could be rapidly improved without excessive inflammatory reaction. On the other hand, it was reported that the micropores affect the mechanical properties of the graft. Kasyanov *et al.* suggested that the mechanical properties of the decellularized tissue have not changed after perforation with a diameter of 50 μm in the case of 714 μm in micropore interval. However, the mechanical properties were largely decreased when the graft was perforated with a diameter of 100 μm and/or a shorter interval.[14] Therefore, it would be important to select the appropriate diameter and distance of the micropores for not only the tissue regeneration but also the preservation of desirable mechanical strength.

The effect of the micropore size on cell infiltration and macrophage polarization has been reported using synthetic polymer scaffolds. Lee *et al.* reported that rapid cell infiltration in micropore structures with diameters of 50, 100, and 200 μm drastically increased the M2 macrophages, as well as overall cell infiltration.[31] In the developed system, macrophage accumulation

subsided due to cell infiltration, suggesting that rapid cell infiltration in decellularized tissue is also desirable for promoting tissue regeneration. Wang *et al.* reported that the micropore size controlled the macrophage polarization, and pores with a diameter of 30 μm induced infiltration of a large number of M2 macrophages into the electrospun scaffold.[11] Christman *et al.* suggested that the pore size affected the macrophage response,[32] and tissue repair was promoted by pores with a diameter of 30–40 μm.[33] We tried to control the micropore diameter of 30 to 40 μm. As a result, the diameter of 24 μm in the decellularized vascular graft was most suitable in terms of reproducibility and fewer damages to the tissues. In the present experiments, the pore size of the decellularized tissue was controlled at 24 μm, and rapid cell infiltration and reduction of the CD68 positive cells were observed in the patterned pore structure. These reports and the present findings suggest that a patterned pore structure with a pore diameter of 24 μm and intervals of 100–250 μm may be optimal for recellularization and tissue regeneration in decellularized grafts. Genetic evaluation would be very useful for understanding macrophage polarization and the phenotype of the infiltrating cells. This research did not mention macrophage polarization in detail, which is a limitation of the study. Nevertheless, it was very meaningful that optimal tissue regeneration in decellularized tissue can be controlled by not only the micropores, but also the intervals. Further studies are required in the future.

5. Conclusion

The results of this study suggest that the patterned pore structure enabled rapid infiltration of host cells into the decellularized vascular graft, and the acute immune response was rapidly silenced. These features are important findings in accelerating tissue regeneration for tissue-engineered vascular grafts.

Author contributions

Atsushi Mahara: conceptualization, methodology, investigation, writing – original draft. Kentaro Kojima: data curation, visualization, investigation Masami Yamamoto: visualization. Yoshiaki Hirano: validation, supervision. Tetsuji Yamaoka: conceptualization, resources, writing – review & editing, funding acquisition, supervision.

Conflicts of interest

There are no conflicts to declare.

Acknowledgements

This work was supported by the Intramural Research Fund of the National Cerebral and Cardiovascular Center (22-2-4) and the S-Innovation Project of the Japan Agency for Medical Research and Development (AMED).

Notes and references

1 S. L. Dahl, A. P. Kypson, J. H. Lawson, J. L. Blum, J. T. Strader, Y. Li, R. J. Manson, W. E. Tente, L. DiBernardo, M. T. Hensley, R. Carter, T. P. Williams, H. L. Prichard, M. S. Dey, K. G. Begelman and L. E. Niklason, *Sci. Transl. Med.*, 2011, **3**, 68.

2 N. L'Heureux, N. Dusserre, A. Marini, S. Garrido, L. de la Fuente and T. McAllister, *Nat. Clin. Pract. Cardiovasc. Med.*, 2007, **4**, 389–395, DOI: 10.1038/ncpcardio0930.

3 J. D. Roh, R. Sawh-Martinez, M. P. Brennan, S. M. Jay, L. Devine, D. A. Rao, T. Yi, T. L. Mirensky, A. Nalbandian, B. Udelsman, N. Hibino, T. Shinoka, W. M. Saltzman, E. Snyder, T. R. Kyriakides, J. S. Pober and C. K. Breuer, *Proc. Natl. Acad. Sci. U. S. A.*, 2010, **107**, 4669–4674, DOI: 10.1073/pnas.0911465107.

4 Y. Y. Gong, J. X. Xue, W. J. Zhang, G. D. Zhou, W. Liu and Y. Cao, *Biomaterials*, 2011, **32**, 2265–2273, DOI: 10.1016/j.biomaterials.2010.11.078.

5 K. Sadtler, K. Estrellas, B. W. Allen, M. T. Wolf, H. Fan, A. J. Tam, C. H. Patel, B. S. Luber, H. Wang, K. R. Wagner, J. D. Powell, F. Housseau, D. M. Pardoll and J. H. Elisseeff, *Science*, 2016, **352**, 366–370, DOI: 10.1126/science.aad9272.

6 B. N. Brown, B. D. Ratner, S. B. Goodman, S. Amar and S. F. Badylak, *Biomaterials*, 2012, **33**, 3792–3802, DOI: 10.1016/j.biomaterials.2012.02.034.

7 S. F. Badylak, J. E. Valentin, A. K. Ravindra, G. P. McCabe and A. M. Stewart-Akers, *Tissue Eng., Part A*, 2008, **14**, 1835–1842, DOI: 10.1089/ten.tea.2007.0264.

8 M. T. Khorasani and S. Shorgashti, *J. Biomed. Mater. Res., Part B*, 2006, **76**, 41–48, DOI: 10.1002/jbm.b.30363.

9 T. Yaguchi, A. Funakobo, T. Okoshi, Y. Noishiki and Y. Fukui, *J. Artif. Organs*, 2002, **5**, 117–122, DOI: 10.1007/s100470200021.

10 K. Doi and T. Matsuda, *J. Biomed. Mater. Res.*, 1997, **34**, 361–370, DOI: 10.1002/(sici)1097-4636(19970305)34:3<361::aid-jbm11>3.0.co;2-j.

11 Z. Wang, Y. Cui, J. Wang, X. Yang, Y. Wu, K. Wang, X. Gao, D. Li, Y. Li, X. Zheng, Y. Zhu, D. Kong and Q. Zhao, *Biomaterials*, 2014, **35**, 5700–5710, DOI: 10.1016/j.biomaterials.2014.03.078.

12 K. Wang, M. Zhu, T. Li, W. Zheng, L. Li, M. Xu, Q. Zhao, D. Kong and L. Wang, *J. Biomed. Nanotechnol.*, 2014, **10**, 1588–1598, DOI: 10.1166/jbn.2014.1849.

13 W. S. Sheridan, O. B. Grant, G. P. Duffy and B. P. Murphy, *J. Biomed. Mater. Res., Part B*, 2014, **102**, 1700–1710, DOI: 10.1002/jbm.b.33138.

14 V. A. Kasyanov, J. Hodde, M. C. Hiles, C. Eisenberg, L. Eisenberg, L. E. F. De Castro, I. Ozolanta, M. Murovska, R. A. Draughn, G. D. Prestwich, R. R. Markwald and V. Mironov, *J. Mater. Sci.: Mater. Med.*, 2009, **20**, 329–337, DOI: 10.1007/s10856-008-3590-3.

15 H. Bergmeister, P. Boeck, M. Kasimir, T. Fleck, F. Fitzal, W. Husinsky, M. Mittlboeck, H. G. Stoehr, U. Losert, E. Wolner and M. Grabenwoeger, *J. Biomed. Mater. Res., Part B*, 2005, **74**, 495–503, DOI: 10.1002/jbm.b.30228.

16 A. Mahara, T. Sakuma, N. Mihashi, T. Moritan and T. Yamaoka, *Colloids Surf., B*, 2019, **181**, 806–813, DOI: 10.1016/j.colsurfb.2019.06.037.
17 H. Yamanaka, T. Yamaoka, A. Mahara, N. Morimoto and S. Suzuki, *Biomaterials*, 2018, **179**, 156–163, DOI: 10.1016/j.biomaterials.2018.06.022.
18 A. Mahara, S. Somekawa, N. Kobayashi, Y. Hirano, Y. Kimura, T. Fujisato and T. Yamaoka, *Biomaterials*, 2015, **58**, 54–62, DOI: 10.1016/j.biomaterials.2015.04.031.
19 C. T. Rueden, J. Schindelin, M. C. Hiner, B. E. DeZonia, A. E. Walter, E. T. Arena and K. W. Eliceiri, *BMC Bioinf.*, 2017, **18**, 529, DOI: 10.1186/s12859-017-1934-z.
20 B. K. H. L. Boekema, M. Vlig, L. O. Damink, E. Middelkoop, L. Eummelen, A. V. Bühren and M. M. W. Ulrich, *J. Mater. Sci.: Mater. Med.*, 2014, **25**, 423–433, DOI: 10.1007/s10856-013-5075-2.
21 J. K. Chai, L. Liang, H. Yang, R. Feng, H. Yin, F. Li and Z. Sheng, *Burns*, 2007, **33**, 719–725, DOI: 10.1016/j.burns.2006.08.039.
22 T. Yu, L. Wen, J. He, Y. Xu, T. Li, W. Wang, Y. Ma, M. A. Ahmad, X. Tian, J. Fan, X. Wang, H. Hagiwara and Q. Ao, *Acta Biomater.*, 2020, **115**, 235–249, DOI: 10.1016/j.actbio.2020.07.059.
23 A. Kriebel, M. Rumman, M. Scheld, D. Hodde, G. Brook and J. Mey, *J. Biomed. Mater. Res., Part B*, 2014, **102**, 356–365, DOI: 10.1002/jbm.b.33014.
24 Y. Xu, D. Li, Z. Yin, A. He, M. Lin, G. Jiang, X. Song, X. Hu, Y. Liu, J. Wang, X. Wang, L. Duan and G. Zhou, *Acta Biomater.*, 2017, **58**, 113–121, DOI: 10.1016/j.actbio.2017.05.010.
25 C. M. Juran, M. F. Dolwick and P. S. McFetridge, *Tissue Eng., Part A*, 2015, **21**, 829–839, DOI: 10.1089/ten.TEA.2014.0250.
26 C. M. Murphy, M. G. Haugh and F. J. O'Brien, *Biomaterials*, 2010, **31**, 461–466, DOI: 10.1016/j.biomaterials.2009.09.063.
27 M. Grabenwöger, F. Fitzal, J. Sider, C. Csekö, H. Bergmeister, H. Schima, W. Husinsky, P. Böck and E. Wolner, *Ann. Thorac. Surg.*, 1998, **66**(Supplement), S110–S114, DOI: 10.1016/s0003-4975(98)00982-5.
28 Y. Zhang, Y. Xu, Y. Liu, D. Li, Z. Yin, Y. Huo, G. Jiang, Y. Yang, Z. Wang, Y. Li, F. Lu, Y. Liu, L. Duan and G. Zhou, *J. Mech. Behav. Biomed. Mater.*, 2019, **90**, 96–103, DOI: 10.1016/j.jmbbm.2018.10.006.
29 J. M. Anderson, A. Rodriguez and D. T. Chang, *Semin. Immunol.*, 2008, **20**, 86–100, DOI: 10.1016/j.smim.2007.11.004.
30 S. Jahnavi, N. Arthi, S. Pallavi, C. Selvaraju, G. S. Bhuvaneshwar, T. V. Kumary and R. S. Verma, *Mater. Sci. Eng., C*, 2017, **77**, 190–201, DOI: 10.1016/j.msec.2017.03.159.
31 B. L. Lee, H. Jeon, A. Wang, Z. Yan, J. Yu, C. Grigoropoulos and S. Li, *Acta Biomater.*, 2012, **8**, 2648–2658, DOI: 10.1016/j.actbio.2012.04.023.
32 K. L. Christman, *Science*, 2019, **363**, 340–341, DOI: 10.1126/science.aar2955.
33 L. R. Madden, D. J. Mortisen, E. M. Sussman, S. K. Dupras, J. A. Fugate, J. L. Cuy, K. D. Hauch, M. A. Laflamme, C. E. Murry and B. D. Ratner, *Proc. Natl. Acad. Sci. U. S. A.*, 2010, **107**, 15211–15216, DOI: 10.1073/pnas.1006442107.

